An Adaptive Sliding Mode Control with Integral Sliding Surface for 3DOF SCARA Manipulators

Jatupon Em-Udom
Thai-Nichi International College, Thai-Nichi Institute of Technology, Bangkok, Thailand
jatupon.emu@tni.ac.th

Kawiwat Amnatchotiphan
Thai-Nichi International College, Thai-Nichi Institute of Technology, Bangkok, Thailand
kawiwat@tni.ac.th (corresponding author)

Received: 17 January 2025 | Revised: 4 March 2025 and 13 March 2025 | Accepted: 17 March 2025

 DOI: https://doi.org/10.48084/etasr.10269

ABSTRACT

This paper presents an adaptive sliding mode control algorithm with an integral sliding surface variable modification for a 3-Degree-Of-Freedom (3DOF) Selective Compliance Articulated Robot Arm (SCARA) with a variable mass at the end-effector. This control technique allows establishing a control law more conveniently compared to conventional sliding mode control methods, as it does not require precise knowledge of the manipulator's dynamic model and does not demand a priori bounded uncertainty or disturbance information. A computational study was carried out to evaluate the performance of the proposed control law and compare it with various motion control techniques, including Proportional-Integral-Derivative (PID) control and traditional sliding mode control. This study used a point-to-point trajectory profile based on a cubic function to assess the tracking performance of different control methods. The computational study involved two scenarios: one without uncertainties and disturbances, and another in which these factors were present. The results show that the proposed method improves joint tracking accuracy over PID control and significantly reduces chattering compared to traditional sliding mode control, both under normal and disturbed conditions, highlighting the effectiveness of the proposed algorithm.

Keywords-3DOF SCARA; adaptive sliding mode control; chattering; uncertainties and disturbances

I. INTRODUCTION

Robotics has revolutionized industries by improving automation precision and productivity. The 3-Degree-Of-Freedom (3DOF) Selective Compliance Articulated Robot Arm (SCARA), known for its simplicity, efficiency, and cost-effectiveness, excels in planar and vertical movements, making it ideal for assembly and automation tasks [1-3]. Its horizontal compliance and vertical rigidity enable precise high-speed operations in tight spaces. A high-performance motion controller, such as the widely used Proportional-Integral-Derivative (PID) controller, ensures accuracy during fast movements [4, 5]. This control method is valued for its simplicity and versatility in position and velocity regulation and minimizes errors to ensure consistent performance under varying conditions. With proper tuning, PID controllers [6] can be adaptable to diverse applications. However, their effectiveness is limited when dealing with parametric uncertainties, disturbances, and highly nonlinear systems [7].

Another well-known technique is fuzzy logic control [8-10], which handles uncertainty and unclear system models but lacks stability guarantees and requires expert-driven trial-and-error in rule design. An alternative approach combines PID control with fuzzy logic [11], mimicking the biological immune system to handle uncertainties and parametric variations. Neural network control [12, 13] excels in complex tasks but lacks stability guarantees, relies on quality data, and risks overfitting, which reduces robustness. However, Sliding Mode Control (SMC) [14-16] ensures stability and reliability, overcoming the limitations of model-free methods such as fuzzy logic and neural networks. Its robustness against nonlinearities, uncertainties, and disturbances makes it ideal for controlling SCARA [17, 18], and the straightforward formulation enables precise and robust control in practical applications.

Conventional Sliding Mode Control (CSMC) ensures robustness but suffers from chattering, gain overestimation, and reliance on precise modeling. Adaptive Sliding Mode Control (ASMC) [19-21] addresses these issues by reducing chattering through adaptive gain tuning, ensuring smoother control and compensating for uncertainties and disturbances, making it more practical than CSMC. This study proposes an ASMC

algorithm for a 3DOF SCARA, building on [22] with an integral sliding surface variable modification. The original work uses only the conventional sliding surface variable, which may cause tracking inaccuracy if the sliding surface variable does not converge to zero. Unlike previous methods [23, 24], it eliminates the need for bounded uncertainty conditions, ensures bounded adaptive gains, and reduces chattering and incomplete convergence. The integral sliding surface variable improves tracking accuracy, allowing joint errors to converge to zero even with residual s values, which is crucial for precise tracking applications.

II. THEORETICAL BACKGROUND

A. Euler-Lagrange Equation for Manipulator

The Euler-Lagrange dynamic model, used in robotic motion control, describes the relationship between applied forces or torques and joint motion. It captures joint dynamics, including viscous and Coulomb friction, as follows [25, 26]:

$$H(q)\ddot{q} + C(q,\dot{q})\dot{q} + F_v\dot{q} + F_c\text{sgn}(\dot{q}) + G(q) = \tau + D \quad (1)$$

where $H(q) \in \mathbb{R}^{nxn}$ is the mass/inertia matrix of the robot manipulator, $C(q,\dot{q}) \in \mathbb{R}^{nxn}$ is the Coriolis-Centripetal force terms, $F_v \in \mathbb{R}^{nxn}$ is the viscous friction matrix, $F_c \in \mathbb{R}^{nxn}$ is the Coulomb friction matrix, $G(q) \in \mathbb{R}^n$ represents the gravitation torque matrix, $\tau \in \mathbb{R}^n$ is the applied torque matrix where each element represents the applied torque component for a particular joint, and $D \in \mathbb{R}^n$ represents disturbance torques for the robot joints. In addition, the signum function, $\text{sgn}(x)$, is defined as

$$\text{sgn}(x) = \begin{cases} 1, & x > 0 \\ 0, & x = 0 \\ -1, & x < 0 \end{cases} \quad (2)$$

This function represents the sign discontinuity of an input variable. Here, q and $\dot{q}$ denote the joint position and velocity, respectively. For Euler-Lagrange systems, especially robot manipulators, several key properties useful for control law design can be found in [27].

Considering a trajectory tracking problem, joint tracking error is defined as $\tilde{q}(t) = q(t) - q_d(t)$ where $q_d(t)$ represents desired joint trajectories with $q_d, \dot{q}_d, \ddot{q}_d \in \mathcal{L}^\infty$. Furthermore, an integral sliding surface variable [28] adopted is defined as:

$$s(t) = \dot{\tilde{q}}(t) + 2\Lambda\tilde{q}(t) + \Lambda^2 \int_0^t \tilde{q}(\tau)\, d\tau \quad (3)$$

where $s \in \mathbb{R}^n$ represents the sliding surface variable, and $\Lambda \in \mathbb{R}^{nxn}$ represents the diagonal positive-definite matrix. Unlike recent studies, the traditional sliding surface variable, given by $s(t) = \dot{\tilde{q}}(t) + \Lambda\tilde{q}(t)$ [14], is used instead of the integral type in (3).

B. Dynamic Model Development

Lagrangian mechanics are used to derive the equation of motion for the 3DOF SCARA manipulator. This energy-based approach is effective for dynamic systems with few degrees of freedom, such as the 3DOF SCARA manipulator. The Lagrangian L is given by [29]:

$$L(q,\dot{q}) = T(q,\dot{q}) - V(q) \quad (4)$$

where $T \equiv T(q,\dot{q})$ denotes the kinetic energy of the system, $V \equiv V(q)$ denotes the potential energy of the system, $q \in \mathbb{R}^3$ represents the generalized coordinate of 3DOF SCARA, and $\dot{q} \in \mathbb{R}^3$ represents the corresponding joint velocity. Figure 1 shows the 3DOF SCARA configuration.

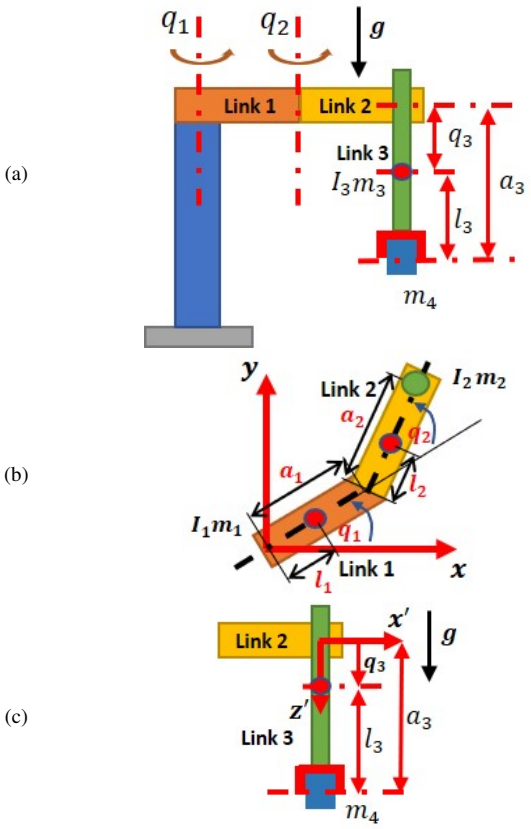

Fig. 1. 3DOF SCARA configuration where the first two degrees of freedom are revolute joint types, and the other degree of freedom is a prismatic joint type: (a) overall configuration, (b) two-planar arm configuration in the horizontal plane for the first two revolute joints, and (c) prismatic joint in the vertical direction.

The robot arm in this figure is a 2R1P type, with two revolute joints (2R) allowing horizontal movement of the first two links and a prismatic joint (1P) providing vertical motion for the final link, which has an additional variable mass m_4.

Unlike the traditional 3DOF SCARA, the total kinetic energy of the 3DOF SCARA with the variable mass m_4, which acts as a picking object and resembling a disturbance, is given by:

$$T = \frac{1}{2}m_1l_1^2\dot{q}_1^2 + \frac{1}{2}m_2a_1^2\dot{q}_1^2 + \frac{1}{2}m_2l_2^2(\dot{q}_1+\dot{q}_2)^2 + m_2a_1l_2Cq_2(\dot{q}_1^2 + \dot{q}_1\dot{q}_2) + \frac{1}{2}m_3a_1^2\dot{q}_1^2 + \frac{1}{2}m_3a_2^2(\dot{q}_1+\dot{q}_2)^2 + m_3a_1a_2Cq_2(\dot{q}_1^2 + \dot{q}_1\dot{q}_2) + \frac{1}{2}m_3\dot{q}_3^2 + \frac{1}{2}m_4a_1^2\dot{q}_1^2 + \frac{1}{2}m_4a_2^2(\dot{q}_1+\dot{q}_2)^2 +$$

$$m_4 a_1 a_2 C q_2 (\dot{q}_1^2 + \dot{q}_1 \dot{q}_2) + \frac{1}{2} m_4 \dot{q}_3^2 + \frac{1}{2} I_1 \dot{q}_1^2 + \frac{1}{2} (I_2 + I_3)(\dot{q}_1 + \dot{q}_2)^2 \quad (5)$$

whereas the total potential energy of this particular robot arm can be written as:

$$V = -m_3 g q_3 - m_4 g q_3 \quad (6)$$

where g denotes the gravitational constant, m_1, m_2 and m_3 are the mass of 3DOF SCARA links 1, 2, and 3, respectively, l_1 and l_2 denote the distances between the corresponding link's center of mass and its axis, a_1 and a_2 represent the lengths of 3DOF SCARA links 1 and 2, respectively, l_3 represents the distance from link 3's center of mass to the object mentioned above, and a_3 is of the form $a_3 = q_3 + l_3$. The equation of motion is given by:

$$\tau_i - \tau_{fi} = \frac{d}{dt}\left(\frac{\partial L}{\partial \dot{q}_i}\right) - \frac{\partial L}{\partial q_i} \quad (7)$$

where τ_i represents the external applied torque and force, depending on the type of each joint such as revolute or prismatic joint, for each generalized coordinate with $i = 1,2,3$. On the contrary, τ_{fi} represents the friction force and torque for each point. According to (1), the equation of motion of 3DOF SCARA can be expressed as:

$$\begin{bmatrix} H_{11} & H_{12} & H_{13} \\ H_{21} & H_{22} & H_{23} \\ H_{31} & H_{32} & H_{33} \end{bmatrix} \begin{bmatrix} \ddot{q}_1 \\ \ddot{q}_2 \\ \ddot{q}_3 \end{bmatrix} + \begin{bmatrix} C_{11} & C_{12} & C_{13} \\ C_{21} & C_{22} & C_{23} \\ C_{31} & C_{32} & C_{33} \end{bmatrix} \begin{bmatrix} \dot{q}_1 \\ \dot{q}_2 \\ \dot{q}_3 \end{bmatrix} + \begin{bmatrix} F_{v11} & 0 & 0 \\ 0 & F_{v22} & 0 \\ 0 & 0 & F_{v33} \end{bmatrix} \begin{bmatrix} \dot{q}_1 \\ \dot{q}_2 \\ \dot{q}_3 \end{bmatrix} + \begin{bmatrix} F_{c11} & 0 & 0 \\ 0 & F_{c22} & 0 \\ 0 & 0 & F_{c33} \end{bmatrix} \begin{bmatrix} \mathrm{sgn}(\dot{q}_1) \\ \mathrm{sgn}(\dot{q}_2) \\ \mathrm{sgn}(\dot{q}_3) \end{bmatrix} + \begin{bmatrix} G_1 \\ G_2 \\ G_3 \end{bmatrix} = \begin{bmatrix} \tau_1 \\ \tau_2 \\ \tau_3 \end{bmatrix} + \begin{bmatrix} D_1 \\ D_2 \\ D_3 \end{bmatrix} \quad (8)$$

where:

$$H_{11} = [I_1 + I_2 + I_3 + m_1 l_1^2 + m_2(a_1^2 + l_2^2 + 2a_1 l_2 C q_2)] + [m_3(a_1^2 + a_2^2 + 2a_1 a_2 C q_2) + m_4(a_1^2 + a_2^2 + 2a_1 a_2 C q_2)]$$

$$H_{12} = [I_2 + I_3 + m_2(l_2^2 + a_1 l_2 C q_2) + m_3(a_2^2 + a_1 a_2 C q_2)] + [m_4(a_2^2 + a_1 a_2 C q_2)]$$

$$H_{13} = 0, H_{23} = 0, H_{31} = 0, H_{32} = 0$$

$$H_{21} = [I_2 + I_3 + m_2(l_2^2 + a_1 l_2 C q_2) + m_3(a_2^2 + a_1 a_2 C q_2)] + [m_4(a_2^2 + a_1 a_2 C q_2)]$$

$$H_{22} = I_2 + I_3 + m_2 l_2^2 + m_3 a_2^2 + m_4 a_2^2$$

$$H_{33} = m_3 + m_4$$

$$C_{11} = -2m_2 a_1 l_2 S q_2 \dot{q}_2 - 2m_3 a_1 a_2 S q_2 \dot{q}_2 - 2m_4 a_1 a_2 S q_2 \dot{q}_2$$

$$C_{12} = -m_2 a_1 l_2 S q_2 \dot{q}_2 - m_3 a_1 a_2 S q_2 \dot{q}_2 - m_4 a_1 a_2 S q_2 \dot{q}_2$$

$$C_{13} = 0, C_{22} = 0, C_{23} = 0, C_{31} = 0, C_{32} = 0, C_{33} = 0$$

$$C_{21} = m_2 a_1 l_2 S q_2 \dot{q}_1 + m_3 a_1 a_2 S q_2 \dot{q}_1 + m_4 a_1 a_2 S q_2 \dot{q}_1$$

$$F_{v11} = F_{v1}, F_{v22} = F_{v2}, F_{v33} = F_{v3}$$

$$F_{c11} = F_{c1}, F_{c22} = F_{c2}, F_{c33} = F_{c3}$$

$$G_1 = 0, G_2 = 0, G_3 = -m_3 g - m_4 g \quad (9)$$

All viscous and Coulomb friction coefficients, F_{vi} and F_{ci} with $i = 1, 2, 3$, are real positive constants. It should be noted that (8) and (9) are nonlinear and coupled differential equations with time-varying parameters.

C. Control Law Design

The adaptive sliding mode control law is given by

$$\tau(t) = -\Gamma s(t) - \eta(t)\mathrm{sgn}\big(s(t)\big) \quad (10)$$

where Γ is a diagonal positive-definite matrix which can be arbitrarily chosen, and $\eta(t)$ is the gain of the control law:

$$\eta(t) = \hat{\xi}_0(t) + \hat{\xi}_1(t)\|\Pi\| + \hat{\xi}_2(t)\|\Pi\|^2 \quad (11)$$

where $\hat{\xi}_0$, $\hat{\xi}_1$, and $\hat{\xi}_2$ represent adaptive variables. The adaptive law for $\hat{\xi}_i$ with $i = 0, 1, 2$ is given by:

$$\dot{\hat{\xi}}_i(t) = \|s(t)\|\|\Pi\|^i - \gamma_i \hat{\xi}_i(t) \quad (12)$$

where $\Pi = \left[\left(\int_0^t \tilde{q} d\tau\right)^T \quad \tilde{q}^T \quad \dot{\tilde{q}}^T\right]^T$ and the initial condition of each adaptive variable is $\hat{\xi}_i(0) \in \mathbb{R}^+$, and $\gamma_i \in \mathbb{R}^+$, which can be arbitrarily chosen. Further stability analysis and theoretical development are omitted here, but more details can be found in [22].

III. COMPUTATIONAL SETUP

This study used a point-to-point trajectory to evaluate the joint trajectory tracking performance of different controllers. The desired trajectory profile for each DOF of the 3DOF SCARA is defined as a cubic trajectory, represented by:

$$q_{id}(t) = c_0 + c_1 t + c_2 t^2 + c_3 t^3, \; i = 1,2,3 \quad (13)$$

where t represents the time variable and $\{c_j\}_{j=0}^3$ are coefficients determined by specifying the initial joint position as well as the final one and velocity of each DOF of the 3DOF SCARA. The initial positions of all joints are set to zero, while the final positions are varied for each joint to clearly highlight the differences in their trajectories. Furthermore, to verify tracking performance under parametric uncertainties and disturbances across diverse controllers, these uncertain parameters are established by using sinusoidal functions. The parametric uncertainty is represented by:

$$m_{4unc} = m_4 + m_{4amp} sin(w_m t) \quad (14)$$

where m_{4amp} is the amplitude variation of the mass m_4 in (4), and w_m is the angular frequency of mass variation. On the other hand, the disturbance D in (1), which represents unexpected external torques/forces, is given by

$$D_i = d_{amp} sin(w_d t), \quad i = 1,2,3 \quad (15)$$

where d_{amp} and w_d are the amplitude and angular frequency of disturbance, respectively. The results of this computational study are provided in the next section. It should be noted that all computational studies were conducted using MATLAB/Simulink 2024a on a system with a 13th Gen Intel®

Core™ i5-13420H processor (2.10 GHz), 32 GB of RAM, and an NVIDIA GeForce RTX 4050 GPU. This computational setup ensures the efficient execution of numerical simulations and control algorithm implementations.

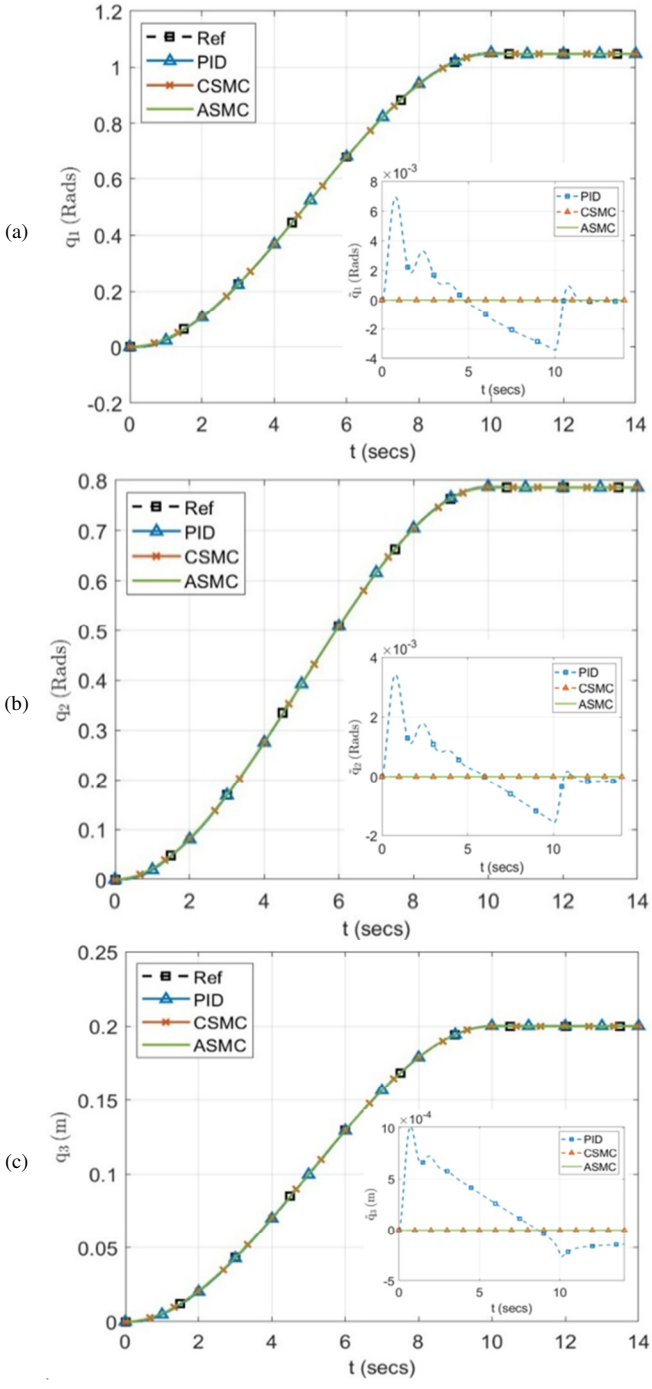

Fig. 2. Trajectory tracking performance without parametric uncertainties and disturbances for PID control (blue line), CSMC (orange line), and ASMC (green line): (a) joint 1, (b) joint 2, (c) joint 3. The inset figures depict the joint tracking errors produced by each control method.

IV. RESULTS AND DISCUSSION

A. 3DOF SCARA without Parametric Uncertainties and Disturbances

Figure 2 shows the performance of the PID control, CSMC, and ASMC, including the reference trajectory. The results indicate that the joint tracking responses of all three control methods align closely with the reference trajectory, demonstrating the overall accuracy of these methods. Furthermore, a more detailed examination reveals that both the CSMC and ASMC provide superior joint tracking precision compared to PID control. This observation is supported by the inset figures in Figure 2, which show the joint tracking errors for the considered control algorithms. These error plots clearly highlight the enhanced performance of the sliding mode-based methods in terms of achieving accuracy and reliable control.

Although the CSMC can deliver impressive tracking performance, it can suffer from chattering when compared to the PID control and ASMC, as shown in Figures 3(a) and 3(b). Figure 3(c) shows that the control input signal $\mathcal{F}_3$ of the CSMC is not affected by the chattering phenomenon, probably due to the simplicity of the dynamic equation governing the 3DOF SCARA in the prismatic coordinate q_3.

In summary, the ASMC demonstrates both exceptional tracking accuracy and immunity to chattering, as confirmed by the computational results. These attributes make ASMC a more appealing control algorithm compared to its conventional counterpart and the PID control, due to its high precision and robust control performance.

B. 3DOF SCARA with Parametric Uncertainties and Disturbances

Figure 4 summarizes the in-silico investigation on the joint tracking performance of the ASMC, CSMC, and PID control with parametric variations and disturbances. The results in this figure indicate that the joint tracking responses obtained by the PID control are significantly affected by uncertainties and disturbances because it cannot maintain its tracking accuracy when compared to the reference trajectory profile. In contrast, the CSMC and ASMC exhibit superior tracking performance even under uncertainty and disturbance conditions.

The inset figures in Figure 4, which illustrate the joint tracking errors for all control methods, also confirm this observation. These error plots demonstrate the superior performance of the sliding mode-based approach, underscoring its ability to deliver both precise and dependable control even under uncertain and disturbing conditions.

Like 3DOF SCARA without uncertainty and disturbance scenarios, the control inputs for the CSMC suffer from chattering, as illustrated in Figures 5(a) and 5(b). However, the control input signal $\mathcal{F}_3$ of the CSMC is not affected by the chattering phenomenon, as shown in Figure 5(c). This can be explained by the same reason as the dynamic system in which uncertainties and disturbances are not present.

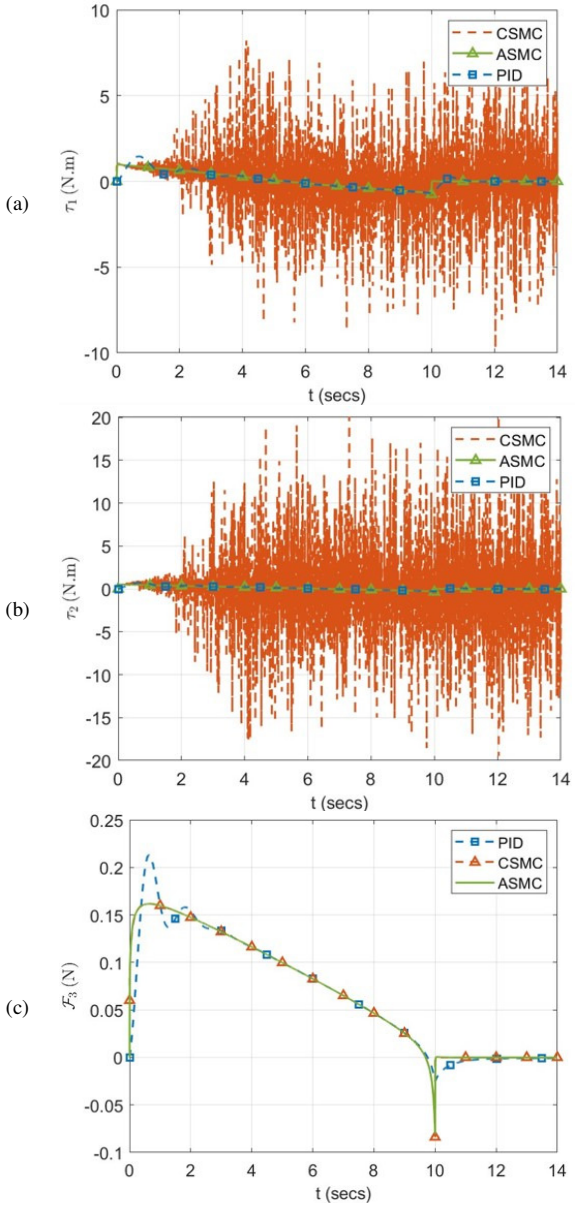

Fig. 3. Control input signals without parametric uncertainties and disturbances for PID control (blue line), CSMC (orange line), and ASMC (green line): (a) joint 1, (b) joint 2, (c) joint 3.

Despite its high tracking performance, CSMC remains susceptible to chattering, primarily due to the use of an overly conservative predefined gain in the discontinuous control input. While this conservative design ensures robustness, it often results in excessive switching activity, which can negatively impact system performance and actuator longevity. Fortunately, this issue can be effectively mitigated by employing the ASMC, where the gain in the discontinuous control input is progressively adapted based on system dynamics, rather than being fixed at an overestimated value. By dynamically adjusting the gain, the ASMC significantly reduces chattering while maintaining robust tracking performance, leading to smoother control inputs.

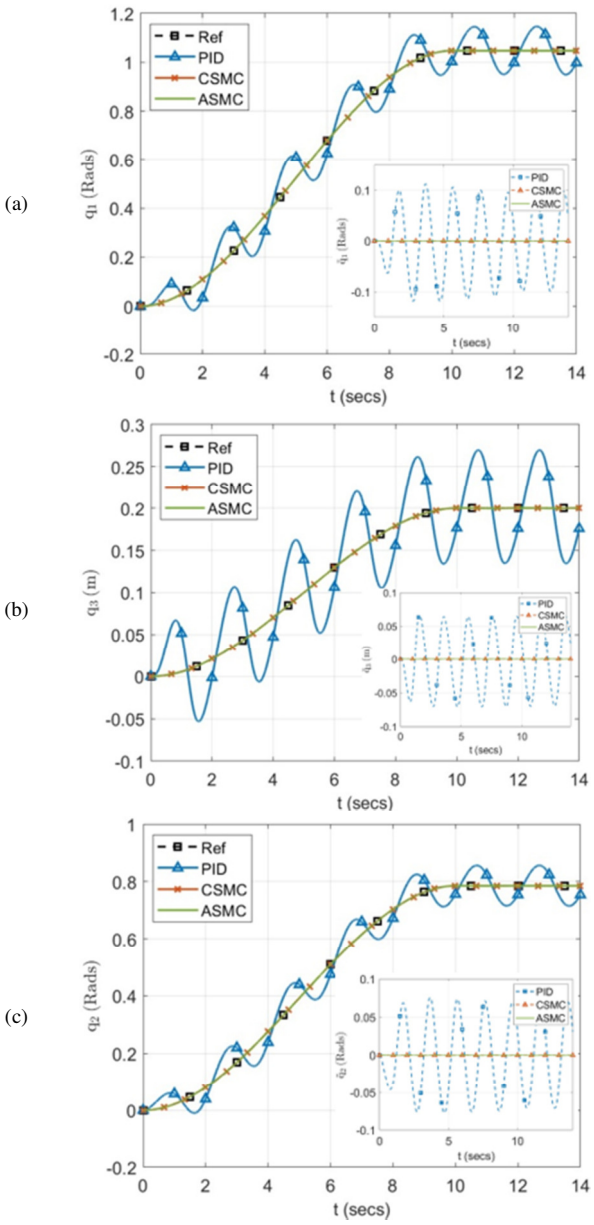

Fig. 4. Trajectory tracking performance with parametric uncertainties and disturbances for PID control (blue line), CSMC (orange line), and ASMC (green line): (a) joint 1, (b) joint 2, (c) joint 3. The inset figures depict the joint tracking errors produced by each control method.

Similar work was carried out in [17, 18]. While their results were promising, these studies focused on CSMC, relying on the robot's dynamic model for control law design. In contrast, our method is more practical, as it does not require precise knowledge of the dynamic model. In [30], an innovative ASMC method was introduced, which employed fuzzy logic control instead of the traditional signum function to mitigate chattering. This approach not only delivers impressive results but also eliminates the need for precise knowledge of the robot's dynamic model.

It is important to note that a continuous trajectory profile is more sophisticated when compared to the point-to-point

trajectory type. However, various forms of continuous trajectory profiles exist, each exhibiting distinct characteristics. As a result, further computational investigation is needed to ensure precise outcome predictions.

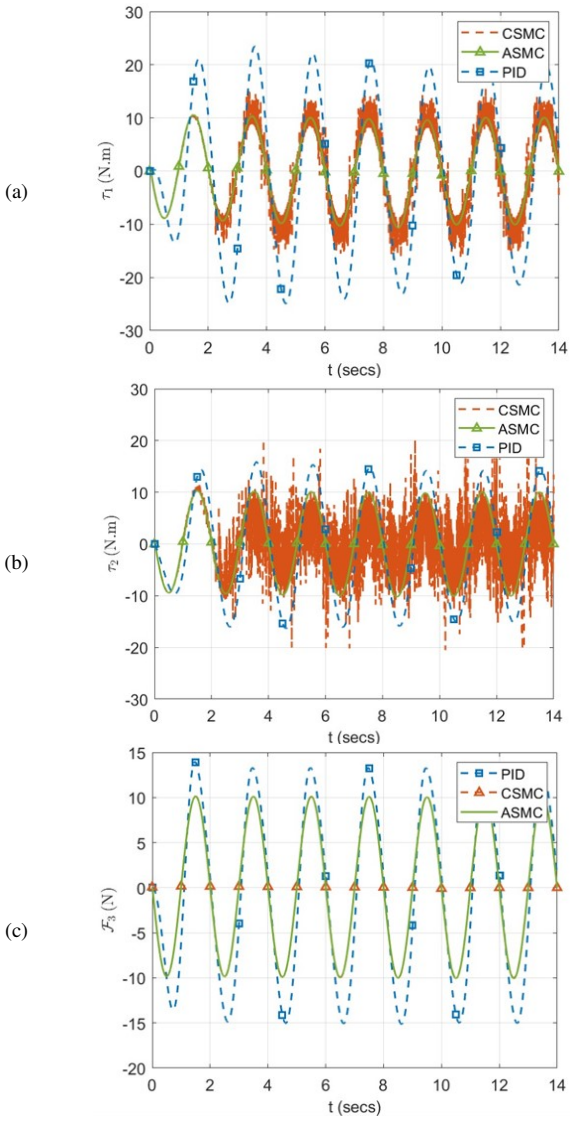

Fig. 5. Control input signals with parametric uncertainties and disturbances for PID control (blue line), CSMC (orange line), and ASMC (green line): (a) joint 1, (b) joint 2, (c) joint 3.

V. CONCLUSION

This study presented an adaptive sliding mode control method with an integral sliding surface variable, inspired by [22], for joint trajectory tracking of 3DOF SCARA manipulators. This method eliminates the need for precise dynamic models or exact bounds of uncertainties, making it simpler and more practical to implement. The computational results show that the proposed method significantly reduces joint tracking errors compared to the PID control while achieving comparable accuracy to the CSMC with much less implementation complexity. Additionally, it minimizes chattering in control inputs, offering smoother performance. These benefits are especially evident under parametric uncertainties and external disturbances, demonstrating its robustness and effectiveness.

This method can be readily extended to the control of a 4-DOF SCARA manipulator, highlighting its scalability. To do so, the dimension of the sliding surface variable vector s in (10) can be increased from 3 to 4, and the diagonal positive-definite matrix Γ in (10) expanded from 3×3 to 4×4. Unlike the CSMC method, which requires precise knowledge of the manipulator's dynamic model, the proposed approach does not rely on the explicit mathematical structure of the 4DOF SCARA manipulator. Future work will involve validating this approach in physical robot manipulators.

REFERENCES

[1] S. Suri, A. Jain, N. Verma, and N. Prasertpoj, "SCARA Industrial Automation Robot," in *2018 International Conference on Power Energy, Environment and Intelligent Control (PEEIC)*, Greater Noida, India, Apr. 2018, pp. 173–177, https://doi.org/10.1109/PEEIC.2018.8665440.

[2] A. Misra, A. Sharma, G. Singh, A. Kumar, and V. Rastogi, "Design and Development of a Low-Cost CNC Alternative SCARA Robotic Arm," *Procedia Computer Science*, vol. 171, pp. 2459–2468, Jan. 2020, https://doi.org/10.1016/j.procs.2020.04.266.

[3] F. Núñez, B. Madrid, J. Chávez, and M. J. Madrid, "SCARA Robot Arm for Disassembly Tasks," in *2024 9th International Conference on Control and Robotics Engineering (ICCRE)*, Osaka, Japan, May 2024, pp. 202–206, https://doi.org/10.1109/ICCRE61448.2024.10589757.

[4] W. Yu and J. Rosen, "A novel linear PID controller for an upper limb exoskeleton," in *49th IEEE Conference on Decision and Control (CDC)*, Atlanta, GA, USA, Dec. 2010, pp. 3548–3553, https://doi.org/10.1109/CDC.2010.5716985.

[5] R. P. Borase, D. K. Maghade, S. Y. Sondkar, and S. N. Pawar, "A review of PID control, tuning methods and applications," *International Journal of Dynamics and Control*, vol. 9, no. 2, pp. 818–827, Jun. 2021, https://doi.org/10.1007/s40435-020-00665-4.

[6] O. Saleem, K. R. Ahmad, and J. Iqbal, "Fuzzy-Augmented Model Reference Adaptive PID Control Law Design for Robust Voltage Regulation in DC–DC Buck Converters," *Mathematics*, vol. 12, no. 12, Jan. 2024, Art. no. 1893, https://doi.org/10.3390/math12121893.

[7] S. H. Tay, W. H. Choong, and H. P. Yoong, "A Review of SCARA Robot Control System," in *2022 IEEE International Conference on Artificial Intelligence in Engineering and Technology (IICAIET)*, Kota Kinabalu, Malaysia, Sep. 2022, pp. 1–6, https://doi.org/10.1109/IICAIET55139.2022.9936755.

[8] S. Huang and D. Yang, "Fuzzy logic controller for a SCARA robot with synchronous network," *International Journal of Computer Applications in Technology*, vol. 10, no. 1–2, pp. 15–26, Jan. 1997, https://doi.org/10.1504/IJCAT.1997.062237.

[9] Y. Oktarina, F. Septiarini, T. Dewi, P. Risma, and M. Nawawi, "Fuzzy-PID Controller Design of 4 DOF Industrial Arm Robot Manipulator.," *Computer Engineering & Applications Journal*, vol. 8, no. 2, 2019.

[10] D. V. Doan, K. Nguyen, and Q. V. Thai, "A Novel Fuzzy Logic Based Load Frequency Control for Multi-Area Interconnected Power Systems," *Engineering, Technology & Applied Science Research*, vol. 11, no. 4, pp. 7522–7529, Aug. 2021, https://doi.org/10.48084/etasr.4320.

[11] O. Saleem, A. Hamza, and J. Iqbal, "A Fuzzy-Immune-Regulated Single-Neuron Proportional–Integral–Derivative Control System for Robust Trajectory Tracking in a Lawn-Mowing Robot," *Computers*, vol. 13, no. 11, Nov. 2024, Art. no. 301, https://doi.org/10.3390/computers13110301.

[12] M. A. Al-Khedher and M. S. Alshamasin, "SCARA robot control using neural networks," in *2012 4th International Conference on Intelligent and Advanced Systems (ICIAS2012)*, Kuala Lumpur, Malaysia, Jun. 2012, pp. 126–130, https://doi.org/10.1109/ICIAS.2012.6306173.

[13] Y. He *et al.*, "Dynamic Modeling, Simulation, and Experimental Verification of a Wafer Handling SCARA Robot With Decoupling Servo Control," *IEEE Access*, vol. 7, pp. 47143–47153, 2019, https://doi.org/10.1109/ACCESS.2019.2909657.

[14] J.-J. Slotine and W. Li, *Applied Nonlinear Control*. Englewood Cliffs, Pearson, 1991.

[15] V. Utkin, A. Poznyak, Y. V. Orlov, and A. Polyakov, *Road Map for Sliding Mode Control Design*. Springer International Publishing, 2020.

[16] K. Cherif, A. Sahbani, and K. B. Saad, "Performance Evaluation of PI and Sliding Mode Control for PMSM in Applications for Electric Vehicles," *Engineering, Technology & Applied Science Research*, vol. 14, no. 4, pp. 15464–15470, Aug. 2024, https://doi.org/10.48084/etasr.7172.

[17] Y. Xu, R. Liu, J. Liu, and J. Zhang, "A novel constraint tracking control with sliding mode control for industrial robots," *International Journal of Advanced Robotic Systems*, vol. 18, no. 4, Jul. 2021, Art. no. 17298814211029778, https://doi.org/10.1177/17298814211029778.

[18] L. A. Soriano *et al.*, "Optimization of Sliding Mode Control to Save Energy in a SCARA Robot," *Mathematics*, vol. 9, no. 24, Jan. 2021, Art. no. 3160, https://doi.org/10.3390/math9243160.

[19] Y. J. Huang, T. C. Kuo, and S. H. Chang, "Adaptive Sliding-Mode Control for NonlinearSystems With Uncertain Parameters," *IEEE Transactions on Systems, Man, and Cybernetics, Part B (Cybernetics)*, vol. 38, no. 2, pp. 534–539, Apr. 2008, https://doi.org/10.1109/TSMCB.2007.910740.

[20] F. Plestan, Y. Shtessel, V. Brégeault, and A. Poznyak, "New methodologies for adaptive sliding mode control," *International Journal of Control*, vol. 83, no. 9, pp. 1907–1919, Sep. 2010, https://doi.org/10.1080/00207179.2010.501385.

[21] I. U. Haq *et al.*, "Neural network-based adaptive global sliding mode MPPT controller design for stand-alone photovoltaic systems," *PLOS ONE*, vol. 17, no. 1, 2022, Art. no. e0260480, https://doi.org/10.1371/journal.pone.0260480.

[22] S. Roy, S. Baldi, and L. M. Fridman, "On adaptive sliding mode control without a priori bounded uncertainty," *Automatica*, vol. 111, Jan. 2020, Art. no. 108650, https://doi.org/10.1016/j.automatica.2019.108650.

[23] T. R. Oliveira, J. P. V. S. Cunha, and L. Hsu, "Adaptive sliding mode control for disturbances with unknown bounds," in *2016 14th International Workshop on Variable Structure Systems (VSS)*, Nanjing, China, Jun. 2016, pp. 59–64, https://doi.org/10.1109/VSS.2016.7506891.

[24] L. Zhang, H. Obeid, and S. Laghrouche, "Adaptive Twisting Controller for Linear Induction Motor Considering Dynamic End Effects," in *2018 15th International Workshop on Variable Structure Systems (VSS)*, Graz, Austria, Jul. 2018, pp. 19–24, https://doi.org/10.1109/VSS.2018.8460238.

[25] L. Zhang, Y. Wang, Y. Hou, and H. Li, "Fixed-Time Sliding Mode Control for Uncertain Robot Manipulators," *IEEE Access*, vol. 7, pp. 149750–149763, 2019, https://doi.org/10.1109/ACCESS.2019.2946866.

[26] S. Zhen, Z. Zhao, X. Liu, F. Chen, H. Zhao, and Y.-H. Chen, "A Novel Practical Robust Control Inheriting PID for SCARA Robot," *IEEE Access*, vol. 8, pp. 227409–227419, 2020, https://doi.org/10.1109/ACCESS.2020.3045789.

[27] B. Siciliano and O. Khatib, "Robotics and the Handbook," in *Springer Handbook of Robotics*, B. Siciliano and O. Khatib, Eds. Springer International Publishing, 2016.

[28] C. H. Lin and F. Y. Hsiao, "Proportional-Integral Sliding Mode Control with an Application in the Balance Control of a Two-Wheel Vehicle System," *Applied Sciences*, vol. 10, no. 15, Jan. 2020, Art. no. 5087, https://doi.org/10.3390/app10155087.

[29] V. S. D. M. Sahu, P. Samal, and C. Kumar Panigrahi, "Modelling, and control techniques of robotic manipulators: A review," *Materials Today: Proceedings*, vol. 56, pp. 2758–2766, Jan. 2022, https://doi.org/10.1016/j.matpr.2021.10.009.

[30] S. Fateh and M. M. Fateh, "Superior Adaptive Fuzzy Sliding Mode Control of Electrically Driven Robot Manipulators," *Iranian Journal of Science and Technology, Transactions of Electrical Engineering*, vol. 47, no. 2, pp. 491–502, Jun. 2023, https://doi.org/10.1007/s40998-022-00582-6.